

Molecular Dynamics Simulations of Deuterium Trapping and Re-emission in Tungsten Carbide[†]

Katharina Vörtler* and Kai Nordlund

Association EURATOM-Tekes, Department of Physics, P.O. Box 43, FIN-00014 University of Helsinki, Finland

Received: June 10, 2009; Revised Manuscript Received: January 5, 2010

Tungsten carbide is exposed to deuterium plasmas in fusion reactors. In this context, studying of the interaction between deuterium and impurities originating from the plasma and tungsten carbide is of scientific interest. Molecular dynamics simulations of cumulative deuterium bombardment with C, W, He, Ne, or Ar impurities on crystalline tungsten carbide were performed with ion energies of 100–300 eV. The temperature was 600 K, and the ion flux was $3.38 \times 10^{28} \text{ m}^{-2} \text{ s}^{-1}$. During the bombardment, the sample surface changed from crystalline to amorphous. Deuterium was trapped in the sample, followed by D₂ accumulation into bubbles, which lead in some cases to a “blistering”-like effect. Annealing of the samples after 5000 impacts for 1 ns showed re-emission of D₂ molecules for the 100 eV bombarded samples and no re-emission for the 300 eV bombarded samples.

Introduction

Tungsten carbide (WC) is a very hard material with a high melting point, and it is commonly used as a substitute for diamond in drilling tools. Due to these features, it is also of interest for applications in fusion reactors. The motivation of studying the interaction of deuterium with WC has been mostly in the context of its fusion reactor material application.^{1–4} However, deuterium and noble gas interaction with WC is also of interest in the manufacturing process of WC films as well as in the controlled sputtering of WC surfaces.

Studying the plasma surface interactions between deuterium and impurities originating from the plasma with WC has a direct application in the context of the next experimental fusion reactor ITER. In ITER, the plasma facing components of the divertor part of the reactor (where the highest heat loads are expected) will consist of carbon fiber composite (CFC) and tungsten. Due to material erosion and migration processes, WC will inevitably form in films in the divertor region during reactor operation. The hydrogen isotopes deuterium and tritium will be the fuel of the fusion reactor confined in a plasma, in which also impurities will be present. The impurities originate from the wall materials, the fusion reaction product helium, and other noble gases that are, for example, used for cooling.⁵ Studying the interaction between deuterium and those impurities with WC is important for the following reasons: (i) Chemical changes in the wall material by hydrogen isotope and impurity bombardment determine, among other things, how fast the wall material degrades during reactor operation. (ii) Studying D re-emission from wall material to the plasma also affects the recycling of unburned fuel. (iii) The T retention in the wall material is, apart from degrading the material's properties, an important factor for ITER; the retention of the hydrogen isotope tritium in the reactor components is a safety criterion for operation. The feasibility of future commercial fusion reactors depends on all three latter mentioned facts.

The interaction of low-energy (1–100 eV) ions with surfaces has also been studied extensively in the context of hyperthermal and sputter etching of materials. Using ions in this range, the etching rates of Si, for instance, can be enhanced compared to equilibrium etching.^{6–9} Garrison et al. showed that this is due to the reactive ions attacking the back sides of loosely bound surface groups leading to bond rupture.^{6,7} We later described how the use of high kinetic energies can enable bond breaking and sputtering even under endothermal conditions by H ions which enter between two bonds and break them.¹⁰ This “swift chemical sputtering” mechanism can be considered as a variety of sputter etching¹¹ or direct abstractive etching,⁹ as discussed in detail in ref 12. However, the swift chemical sputtering mechanism is special in that it is endothermal, whereas the other mechanisms are usually considered to be exothermal.¹³

Generally, solid materials degrade due to hydrogen accumulation, where the trapped hydrogen can form voids, bubbles, and blisters.¹⁴ Experiments of deuterium retention in WC and tungsten–carbon mixed films have been performed in refs 2, 4, and 15. The re-emission of D in WC has been studied in refs 1 and 3. However, there exists a lack of comparison of experimental and simulation data, which also includes the chemical processes. The reasons are simulation difficulties arising due to the experimental value of the D flux, which restricts the system size and therefore the realization of realistic simulations. Therefore, a direct understanding of the trapping and re-emission mechanisms of D in WC has not yet been obtained.

Another interesting feature of energetic D implantation into tungsten is the formation of blisters on its surface.¹⁶ This effect is also seen if carbon is present in the tungsten matrix.^{17–19} A “blister” is a void or bubble close to the sample surface.¹⁴ As blistering, we refer in this work to a rupture in the sample leading to an expanding void. This process is also sometimes called flaking or exfoliation. The mechanism of blister formation in tungsten is not yet fully understood, although both experiments¹⁷ and FEM simulations²⁰ have been performed to tackle this problem. Recent experiments indicate that diffusion processes of D in tungsten are responsible for forming blisters.^{19,21}

[†] Part of the “Barbara J. Garrison Festschrift”.

* To whom correspondence should be addressed. E-mail: katharina.vortler@helsinki.fi.

Only one atomistic simulation study of deuterium bombardment on tungsten carbide has been performed earlier.²² Molecular dynamics (MD) simulations using chemical reactive interaction models are suitable to study the chemical reactions of plasma surface interactions on the atomic level. This work is the first MD study focusing on deuterium trapping and re-emission in tungsten carbide. Moreover, chemical and structural changes in the material are studied in detail. In contrast to Träskelin et al., who focus on the carbon erosion of tungsten carbide under deuterium bombardment,²² we consider the effect of plasma impurities, a reactor relevant temperature of 600 K,²³ higher fluence, and larger system sizes. In this work, we performed MD simulations of cumulative deuterium bombardment with C, W, He, Ne, or Ar impurities on crystalline tungsten carbide with ion energies of 100–300 eV, that is, in the low-energy regime with the highest carbon sputtering yield.²²

This work is organized as follows. In the next section, we describe the simulation method. In the Results and Discussion section, we give special attention to the structural changes during bombardment. We depict the deuterium trapping and re-emission during bombardment and during heating of the sample after the bombarding process is finished. Moreover, the accumulation of noble gas atoms in the sample is presented, and finally, we give the conclusions.

Method

The bombardment simulations were run with the MD code PARCAS²⁴ using a reactive bond order potential for the WCH system, which can reasonably describe both pure elements and compounds.²⁵ The interaction models used between the noble gas (He, Ne, and Ar) and W, C, and D atoms were pair potentials of the Ziegler–Biersack–Littmark (ZBL) type.²⁶

The initial simulation cell was a perfect crystalline hexagonal WC structure. It consisted of $8 \times 5 \times 14$ unit cells along the [1000], $[2\bar{1}10]$, and [0001] surfaces, equivalent to 2240 atoms. The cell size corresponded to about $23.4 \times 25.3 \times 39.5$ Å. Initially, this simulation cell was equilibrated at 600 K and 0 pressure using Berendsen temperature and pressure control²⁷ and periodic boundary conditions²⁸ in three dimensions. A surface was created by fixing the two bottom-most located atom layers that mimic an underlying bulk and equilibrating the cell using temperature control and periodic boundaries in the x and y directions. Using the latter method, simulation cells with carbon ((0001)-C)- and tungsten ((0001)-W)-terminated surfaces were created.

The cumulative bombardment simulations were performed using electronic stopping for energetic atoms in the sample (no electronic slowing down was considered for eroded atoms). Simulation with pure (100%) deuterium as the bombarding ion and impurity bombardment with 90% deuterium and 10% C, W, He, Ne, or Ar were performed. Both C- and W-terminated surfaces were used for bombardment. We considered ion energies of 100, 200, and 300 eV. For comparison, pure (100%) C impacts with 100 eV and pure (100%) Ar impacts with 300 eV were performed on W-terminated surfaces. The ion flux was $3.38 \times 10^{28} \text{ m}^{-2} \text{ s}^{-1}$ in all bombardment simulations.

Before each bombardment, the simulation cell was randomly shifted in the x and y directions in order to obtain a uniformly bombarded sample, taking periodic boundaries into account. In the simulations with impurities, the bombarding ion species was randomly determined (90% deuterium; 10% impurity ion). The bombarding ion was placed 5 Å above the cell (a distance larger than the potential cutoff) and bombarded toward the center of the cell in an angle normal to the surface. During the bombard-

ment simulations, temperature control was applied on the cell borders in the x and y directions and on the bottom of the cell in the z direction. The temperature was scaled in a region of 5 Å thickness. The temperature scaling on the five cell borders was used as a damping mechanism for elastic waves. We have previously systematically evaluated the effect of this kind of damping on sputtering and damage production. We found that with system sizes comparable to the present work, the result is not affected by the damping. The simulation time of the temperature scaling on the borders was 3 ps. In this approach, it is assumed that most of the physically and chemically relevant processes on the surface such as sputtering or heat spikes take place in the first 3 ps of the simulation. In the following 2 ps, first, the simulation cell was quenched to the initial temperature (600 K) with a rate of 5.0 K/fs, and second, the cell was equilibrated at 600 K using temperature control (for all atoms in the cell and sputtered/emitted atoms). This cell was then used for the next ion bombardment (taking out of the simulation system possible eroded atoms and atoms that were implanted deeper than the cell boundaries in the z direction). We performed 1000–5000 ion impacts for each considered ion energy, surface, and (mixed) ion species. This corresponds to an ion fluence of 1.69×10^{20} to $8.45 \times 10^{20} \text{ m}^{-2}$.

During the simulation, if an atom or atom cluster was no longer bonded to the surface of the sample (either directly or by its neighbors), it was considered eroded. The D₂ re-emission yields were obtained by averaging the number of released D₂ molecules that were cumulatively obtained during bombardment over the number of ion impacts (the 1 σ standard error of the average was calculated accordingly).

After the bombardment simulations, changes in the crystalline structures were analyzed. The coordination numbers (number of nearest neighbors) with the number of corresponding atom neighbor species were determined using the potential cutoffs of ref 25. A perfect bulk tungsten carbide structure has a coordination number of 6 for C (with 6 W neighbors) and 14 for W (with 6 C and 8 W neighbors). Analyzing the coordination numbers for all atoms in the bombarded sample allowed us to determine the number of sp² and sp³ hybrid C atoms (corresponding to coordination numbers 3 and 4), D₂ molecules, and C-bonded D in the sample, as well as changes in bonding. No interaction between noble gas atoms and C, W, and D atoms in the sample was assumed in this analysis (zero cutoff).

The final simulation cells after 5000 impacts of 100 eV of 100% D, 100 eV of 90% D and 10% C, 300 eV of 90% D and 10% Ar, and 300 eV of 90% D and 10% W were heated to an annealing temperature (600–2000 K) with a rate of 5.0 K/fs. In the following, the cells were equilibrated at the annealing temperature using temperature control. The simulation time for the latter procedure was 1 ns, followed by an analysis for eroded atoms and clusters. Before analyzing changes in bonding after annealing, the sample was cooled down back to 600 K for 1 ps (rate: 10.0 K/fs).

Results and Discussion

Changes in the Structure during Bombardment: Amorphization. Amorphization of the sample was observed during the bombardment process, where two different effects were seen with ion energies of 100 and 300 eV. The distinct behavior at those energies was observed regardless of the presence of impurities on both C- and W-terminated surfaces. The two effects are illustrated in Figure 1. The first effect was observed with bombardment energies of 100 eV. During the bombardment process, the sample becomes gradually amorphous atom line

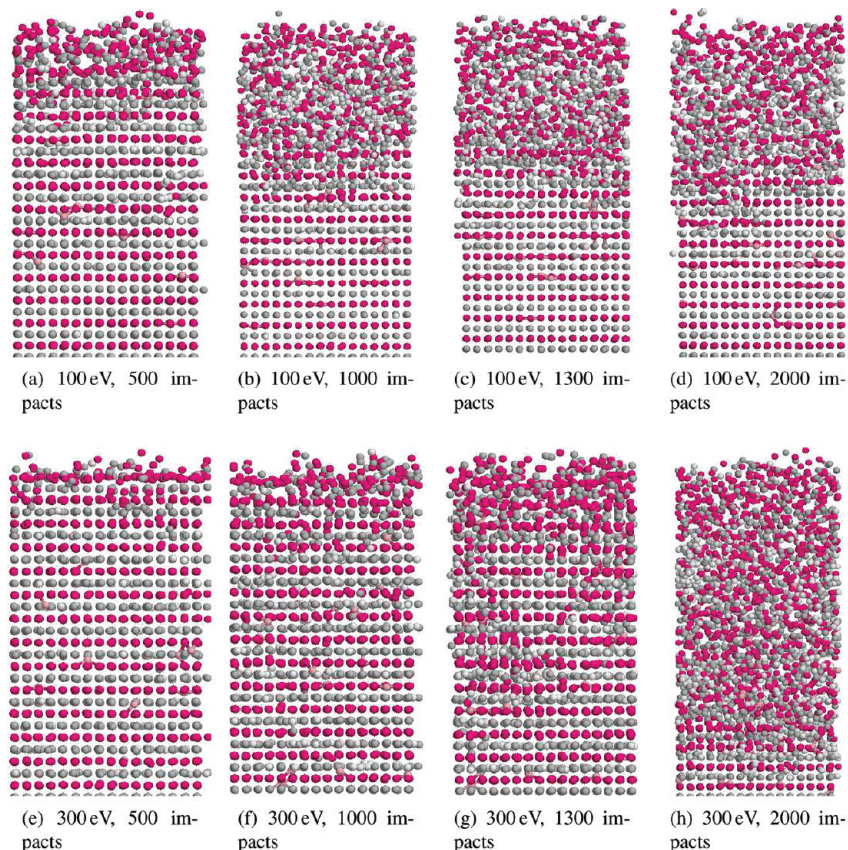


Figure 1. Snapshots of the sample after deuteration with He impurities on (0001)-W; the sample after (a) 500, (b) 1000, (c) 1300, and (d) 2000 ion impacts with 100 eV and (e–h) after ion impacts with 300 eV. The light gray spheres represent D atoms, the light pink He, the dark gray C, and the magenta ones W atoms. The figures show the projection of a full 3D cell into a 2D plane.

by atom line, starting from the surface. As an example, Figure 1a–d shows four snapshots of 100 eV deuteration with He impurities on W-terminated WC. After 500 ion impacts (Figure 1a), about 7 atom layers of the surface show amorphization, and after 2000 impacts (Figure 1d), approximately the upper half of the sample has become amorphous. The second effect was seen with impact energies of 300 eV, illustrated in Figure 1e–h, where, as an example, the bombarding process of 300 eV impacts with deuterium and He impurities on W-terminated WC is shown. After 500 impacts (Figure 1e), the top damage layer is 3 atom layers thick. After 1300 impacts, amorphization is observed in the lower third of the sample. In the following, the crystal structure of the upper two-thirds of the sample collapses, and roughly the whole sample is amorphous after 2000 impacts.

With the help of Figure 1, one can compare the bombardment processes with impact energies of 100 and 300 eV. The top surface layers of the sample are less damaged by 300 eV than those by 100 eV ions after 500 and 1000 impacts. Comparing the snapshots after 1300 and 2000 impacts, more amorphization of the sample by 100 eV ions than by 300 eV ions is seen after 1300 impacts, while after 2000 impacts, the opposite effect is observed.

The latter-described amorphization process was observed regardless of the bombarded surface; only marginal differences in the amount of amorphization in the sample were observed. Comparing the bombardment of pure deuterium and deuterium with impurities, only a marginal difference was seen in the gradual amorphization process by 100 eV ions; however, in the collapsing effect by 300 eV ions, less amorphization was observed in pure deuterium impacts than deuterium with C, W,

and noble gas impurities, and the collapsing of the structure was seen a few hundreds of impacts earlier for simulations with impurities. Only marginal differences in the processes were seen comparing the different impurity bombardments with each other.

The effect seen by impacts with 200 eV ions is similar to the collapsing amorphization by 300 eV ions. However, earlier collapsing (about 500 impacts) of the crystal structure was seen by impacts with 200 eV ions than by 300 eV.

The “gradual amorphization” process starting from the surface for 100 eV ion bombardment described in this section has been observed numerous times by Rutherford backscattering spectroscopy (RBS) in other materials.^{29–31} We cannot rule out the possibility that thermally activated defect migration or recombination would, for typical experimental fluxes (which are much lower than the flux in the current simulations), slow down the amorphization. However, our results will, in any case, be relevant for low enough temperatures or high enough incoming ion fluxes in which significant defect migration cannot take place.

To sum up, a gradual and a collapsing amorphization process was observed depending on the energy of the bombarding ions. However, the result is similar after a few thousand impacts, amorphization of the sample.

Deuterium Trapping and Blistering. The last section showed only marginal differences regardless of whether the sample was originally C- or W-terminated. Therefore, for the bombardment with more than 2000 impacts, only W-terminated samples were considered. Moreover, only Ar was used of the noble gases since it has the most dramatic effect.

Continued bombardment showed further D₂ accumulation in the sample; D₂ bubbles were formed in the material by the high-

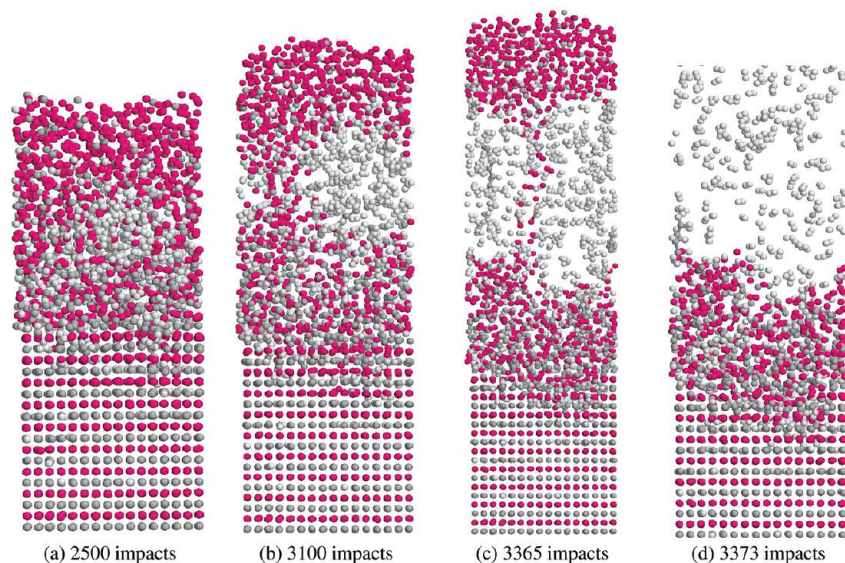


Figure 2. Snapshots of D₂ bubble formation after (a) 2500 and (b) 3100 ion impacts with 90% D and 10% W (100 eV) on W-terminated tungsten carbide. In (c), after 3365 impacts, a separate layer containing D₂ molecules and hydrocarbons is formed (blister). In the following, the top of the sample flew off (flaking) (d) after 3373 bombardments. The light gray spheres represent D atoms, the dark gray C, and the magenta ones W atoms. The figures show the projection of a full 3D cell into a 2D plane.

TABLE 1: Number n of Atoms Having Coordination Numbers 3, 4, and 6 for C and 14 for W, Atomic Percentages, and z Length of Sample of W-Terminated WC^a

	initial	D pure	C mixed	W mixed	D pure	W mixed	Ar mixed	C pure	Ar pure
fluence (10 ²⁰ ions m ⁻²)	0	8.45	8.45	5.68	6.68	8.45	8.45	8.45	8.45
n of impacts	0	5000	5000	3365	3953	5000	5000	5000	5000
ion energy (eV)		100	100	100	300	300	300	100	300
n 14 coord. W atoms	960	303	320	426	27	63	24	586	17
n all W atoms	1120	1120	1106	1440	1120	1537	998	1079	491
ratio 14 coord./all W (%)	87.50	27.05	28.93	29.58	2.41	4.10	2.40	54.31	3.46
n 3 coord. C atoms	80	310	396	237	479	407	415	215	98
n 4 coord. C atoms	0	127	147	154	319	263	230	145	55
n 6 coord. C atoms	1040	447	458	545	48	39	24	846	50
n all C atoms	1120	1021	1148	1051	1043	928	822	1330	246
ratio 3 coord./all C (%)	7.14	30.36	34.49	22.55	45.93	43.86	50.49	16.16	39.84
ratio 4 coord./all C (%)	0	12.43	12.80	14.65	30.58	28.34	27.98	10.90	22.36
ratio 6 coord./all C (%)	92.86	43.78	39.90	51.86	4.60	4.20	2.92	63.61	20.32
ratio C versus C + W (%)	50.00	47.69	50.93	42.19	48.22	37.65	45.16	55.21	33.38
ratio W versus C + W (%)	50.00	52.31	49.07	57.81	51.78	62.35	54.84	44.79	66.62
z length of sample (Å)	39.46	49.61	49.29	82.14	118.71	89.25	46.77	44.60	17.29

^a For comparison, the initial cell is given in the second column. The fluence in the table is shortly before blistering in the case of pure D impacts with 100 eV and mixed (90% D and 10% W) impacts with 300 eV.

flux D impacts. In the case of 300 eV 100% D and 100 eV 90% D, 10% W impacts, this D₂ accumulation led to the separation of a D₂ layer, which also contained hydrocarbons and a tungsten-rich top layer (due to preferred C erosion^{22,32} and/or the mixed W bombardment). This resulted in a blistering-like effect; the top layer was separated by the gas and flew off. Snapshots of the latter-described mechanism are given in Figure 2 (for 100 eV 90% D, 10% W impacts). The fluence when blistering occurred is given in Table 1; the simulation was stopped in this case. In the table, also the thickness (z value) of the simulation cell at the blistering fluence is given. The thickness value of about 119 Å after bombardment with 100% D at 300 eV is due to the accumulation of D in the sample. Our blistering effect and blisters seen in experiment are discussed later in this section.

The number of trapped deuterium atoms in W-terminated tungsten carbide samples depending on the ion fluence is given in Figure 3. It can be seen that for the 100 eV 100% D and 90% D, 10% C impacts, a saturation of 400–500 D atoms in the sample was reached after about 1000 impacts. For 100 eV

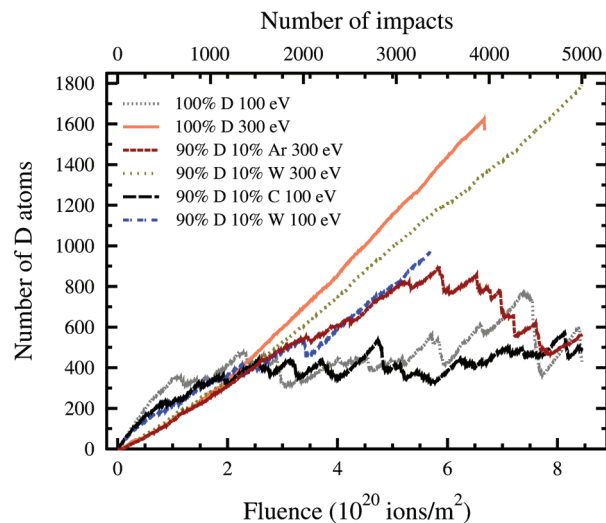


Figure 3. Fluence dependency on deuterium trapping in W-terminated WC samples.

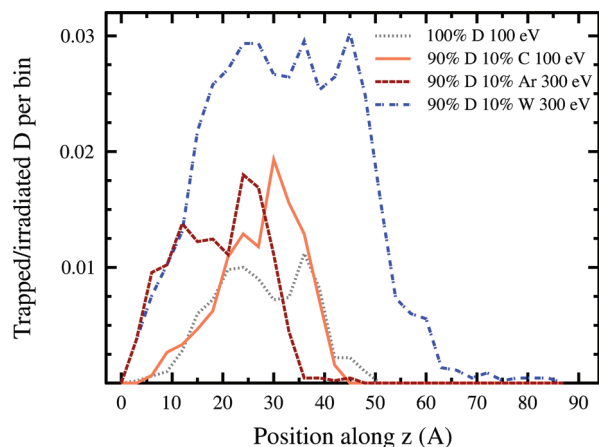


Figure 4. The ratio of the number of trapped D in W-terminated WC over the number of incident D atoms after a fluence of $8.45 \times 10^{20} \text{ m}^{-2}$ (corresponding to 5000 impacts). The ratio of trapped/incident D atoms per bin (bin width 3 Å) per z position in the sample is given.

90% D, 10% W, no saturation was reached, and blistering occurred after a fluence of $5.68 \times 10^{20} \text{ ions m}^{-2}$. Moreover, blistering was observed for 300 eV pure D bombardment after $6.68 \times 10^{20} \text{ ions m}^{-2}$. Linearly increasing D trapping was seen for 300 eV of 90% D, 10% W. The mixed Ar bombardment (90% D, 10% Ar) with the same ion energy showed linear growth of the D in the sample until a fluence of about $5.5 \times 10^{20} \text{ ions m}^{-2}$. By continued bombardment, the number of D atoms in the sample decreased to about the same value for 100 eV of 100% D and 90% D, 10% C at the final ion fluence. Note that ions implanted deeper than the cell boundaries were discarded during the simulations. The here-presented values can be understood as the number of D atoms in a thin film with the size of the z value (thickness) of the simulation box (the final z lengths of those boxes are given in Table 1).

The D depth profile (the number of trapped over incident D) over the z length of the sample after an ion fluence of $8.45 \times 10^{20} \text{ ions m}^{-2}$, corresponding to 5000 impacts, is illustrated in Figure 4. One can see that for the 300 eV 90% D, 10% W bombarded sample, most of the D is present deeper than 30 Å in the sample. From 0 to 10 Å in the z position, the number of D atoms is about the same for both 300 eV bombarded samples (with W and Ar impurities). However, due to higher erosion and no W deposition, the 10% Ar bombarded sample is much smaller in the z dimension and therefore cannot hold an equal number of D as the 10% W bombarded one. The length of the 100 eV bombarded samples (100% D and 90% D, 10% C) is almost the same (Table 1), and the shapes of the profile resemble each other in most z values, although the depth profile suggests a higher number of D for the 10% C bombarded sample. This is indeed reported in a detailed evaluation of the number of trapped D in the sample (Table 2). The high sample thicknesses in the W cobombarded cases are due to both W deposition and D trapping, as reported in the number of W atoms (Table 1) and D atoms in the samples (Table 2).

In the following, the chemistry of the trapped D was analyzed after 5000 impacts, or shortly before the blistering occurred (Table 2). Special attention was paid to the number of trapped D_2 molecules and to D atoms which were bonded to C atoms in the sample. The data in Table 2 show a high D_2 molecule content in the samples shortly before blistering. This is in agreement with the observation of D_2 bubble/layer formation before the top of the sample was blistered. Moreover, the general trend in the data shows that more than 50% of the trapped D

TABLE 2: Evaluation of the Number n of Trapped D_2 Molecules and C-Bonded D in W-Terminated WC^a

	D pure	C mixed	W mixed	D pure	W mixed	Ar mixed
fluence ($10^{20} \text{ ions m}^{-2}$)	8.45	8.45	5.68	6.68	8.45	8.45
n of impacts	5000	5000	3365	3953	5000	5000
ion energy (eV)	100	100	100	300	300	300
n trapped D_2 molecules	72	109	309	513	618	149
n C-bonded D	142	153	142	390	383	157
n trapped D in sample	430	493	972	1573	1789	563
ratio D_2 /trapped D (%)	33.49	42.22	63.58	65.23	69.09	52.93
ratio C-bonded/trapped D (%)	33.02	31.03	14.61	24.79	21.41	27.89
trapped/incident D (%)	8.60	10.96	32.05	39.79	39.76	12.51

^a The ratio of the number of trapped D over the number of bombarded D is given. The fluence in the table is before blistering in the case of pure D impacts with 100 eV and mixed (90% D and 10% W) impacts with 300 eV. The ion flux was $3.38 \times 10^{28} \text{ m}^{-2} \text{ s}^{-1}$.

atoms are in D_2 molecules in the 300 eV bombarded samples while less than 30% are bonded to C. This is also true in the 100 eV mixed W bombarded sample. In the 100 eV of 100% D sample, the number of C-bonded D and D in D_2 is about the same. In the 90% D and 10% C bombarded sample, the number of D in D_2 molecules is about 10% larger than the number of C-bonded D. To summarize, the number of C-bonded D was never in the majority in our bombarded samples (after the given fluence in Table 2 using an ion flux of $3.38 \times 10^{28} \text{ m}^{-2} \text{ s}^{-1}$). If re-emission of D during the bombardment (see next section) is low, in prolonged bombardment, D_2 molecules are favored in the samples; these were seen to accumulate into bubbles.

The observation of a D_2 layer before blistering suggests that the rupture is linked to the D_2 gas pressure, which exerts a force in the z direction. We expected that blistering would occur if the irradiated sample of 300 eV of 90% D, 10% W after 5000 bombardment were heated (structure given in Table 1), since then the D_2 gas pressure is higher. This is due to the fact that its D_2 /all D content (69.09%; see Table 2) is larger than the one in the two blistered samples shortly before their blistering occurred. Indeed, heating of this sample for 1 ns showed blistering for temperatures of 1000 K and higher. In this case, the movement of the D_2 molecules was sufficient to separate the top layer of the sample. On the other hand, annealing at 600 and 800 K showed no blistering nor D re-emission. Only the motion of the D_2 molecule within the sample was seen as well as lifting of the top due to faster motion of D_2 at 800 K, but no layer separation was observed. We conclude that blistering can occur if a sufficient amount of D_2 molecules is present in the sample. No blistering for 100% Ar and C bombardment was observed.

The blisters seen in the experiments by Fukumoto et al.¹⁹ and Shu et al.²¹ (having lower D fluxes than in the present study), which are linked to diffusion of D in tungsten, cannot be explained by our blistering simulations. Diffusion processes of D in tungsten or WC cannot be simulated with MD due to limited simulation times. However, the cited experiments deal with initially pure W, and there is no reason to assume a priori that migration of D in W or WC is comparable. Moreover, our blistering effect is due to the high D flux, as discussed later.

The structure of the sample was analyzed after 5000 impacts or shortly before the blistering occurred. The coordination

numbers of all atoms in the sample were analyzed, as well as the W and C percentages (Table 1). Data of the initial cell are included in the table for comparison. It can be concluded that the majority of the initial tungsten carbide six-coordinated C changed to sp^2 and sp^3 bonding. Of those, C–C bindings were significantly formed in all bombardments with deuterium; for comparison, for pure C and Ar bombardment, this was not the case. Furthermore, the majority of the 14-coordinated W changed to lower coordination numbers. This indicates porosity due to trapped D (see Table 2) and other noble gas accumulation. We can conclude that the original crystalline tungsten carbide structure was destroyed during the bombardment process.

We now discuss how the D trapping seen in our simulations can be compared to experimental data. Direct comparison to experiments cannot be made since the ion flux in our simulations is orders of magnitude higher than experimental fluxes. On the other hand, the experimental fluence is much higher than that in our simulations. Moreover, as already mentioned, diffusion processes of D in WC cannot be simulated.

Kimura et al.³ reported that D trapping depends on interstitial sites and carbon vacancies in crystalline WC. However, we had a much higher D flux, and the crystalline structure was destroyed during bombardment. Alimov² observed trapping of atomic D in WC; no D_2 molecules were formed using an ion flux of $\sim 10^{18} \text{ m}^{-2} \text{ s}^{-1}$, which is 10 orders of magnitude smaller than our flux. Moreover, Alimov did not observe blisters even though higher fluences were used. This does not contradict our observation of a blistering-like effect since for our layer separation, a sufficiently high content of D_2 was needed. The pressure of the steady-state D concentration is responsible for the rupture of the sample. We would expect, on the basis of our simulations, that experiments using higher D fluxes would also show blisters.

We want to add that our blistering is an effect on an atomistic scale; our blisters were much smaller in thickness than those experimentally observed, for example, in tungsten. Our blister (the lifting of the top layer of the sample due to a D_2 -rich layer) can be seen as the center of the experimentally observed blister cup, which is bound to the surface.

Deuterium Re-emission. As already mentioned in the previous section, D_2 re-emission was observed during the bombardment process. The D_2 re-emission yields obtained during bombardment are given in Figure 5. The mixed W bombardments had the lowest D_2 re-emission yields (Figure 5 a). In general, the highest D_2 re-emission was observed during 100 eV bombardment for pure D, while there was hardly any D_2 re-emitted during 300 eV bombardment. The only exception is the D_2 -emission yield for the 300 eV 10% Ar impacts on the W-terminated surface, which is as high as the 100 eV 10% Ar yield on the W-terminated surface (Figure 5b). Since Ar has a relatively high mass compared to D, 300 eV Ar implantation resulted in high W and C erosion of the surfaces (see the z length of the sample in Table 1, which is similar to the 100 eV impacts for pure D and mixed C), and D_2 could escape from the sample during bombardment.

In the following, D re-emission was studied after the bombardment of the samples was completed. The number of re-emitted D versus time for the 100 eV pure D and mixed C bombarded samples is shown in Figure 6. Annealing temperatures from 600 to 2000 K were considered. The 100% D bombarded sample contained 430 D atoms before annealing. Heating the sample to 600–1000 K showed a saturation in the number of re-emitted D after approximately 0.3 ns, and annealing temperatures 1500–2000 showed no saturation (Figure 6a). Analysis of the D_2 content in the total D re-emitted atoms showed that up to 1000 K, almost all re-emitted D was

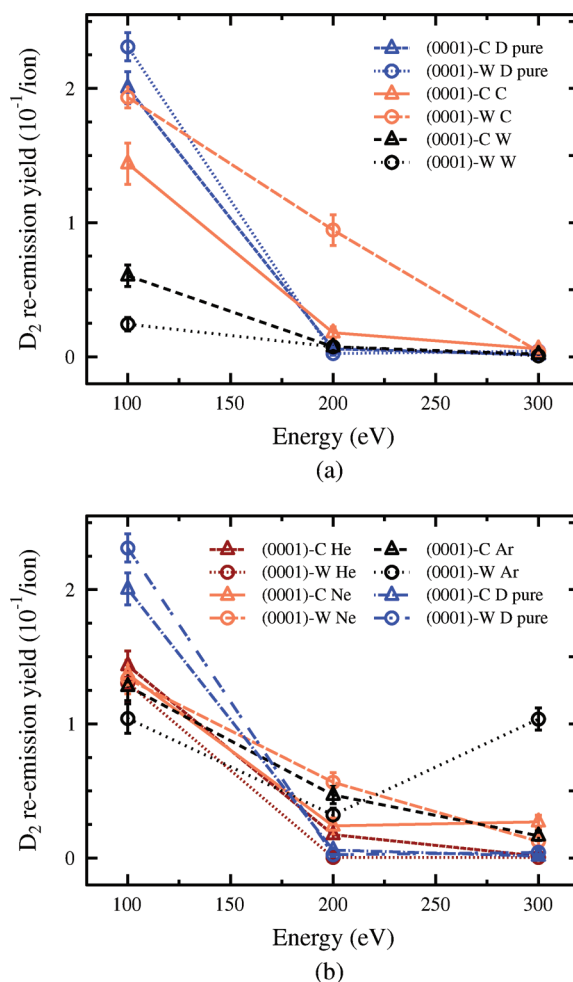


Figure 5. D_2 re-emission yields for bombardment with 100% (pure) D and 90% D, 10% C or W impurities (a) and 100% (pure) D and 90% D, 10% He, Ne, or Ar impurities (b) (0001)-W (W-terminated) and (0001)-C (C-terminated) WC surfaces.

in the form of D_2 molecules (Table 3). Examining the migration path and bonding for 600 K revealed that all re-emitted D_2 existed as molecules in the sample before re-emission. Since the deepest re-emitted D_2 was 20 Å into the sample, we conclude that D_2 is highly mobile in WC.

The number of re-emitted D versus time for the 100 eV 90% D, 10% C bombarded sample is shown in Figure 6b. Before annealing, the sample contained 493 D atoms. It is interesting to note that more D was re-emitted at 800 K than at 1000 K. No saturation effect was seen during the 1 ns annealing time. Detailed information of the number of emitted D_2 is given in Table 4; all D was re-emitted as D_2 . The analysis of the D bonding after heating is also given in Table 4. Comparing the number of re-emitted D_2 molecules, D_2 in the sample, and the number of D in the initial cell shows that 8 out of 9 D_2 for 600 K, 17 out of 19 D_2 for 1000 K, and 29 out of 31 D_2 for 800 K existed as molecules in the sample before re-emission. Analysis of the migration path showed that the deepest re-emitted D_2 was initially 25 Å in sample.

The data in Table 4 also shows that with increasing temperature, the number of C-bonded D increased in the sample. This effect is especially dominant for 1000 K and may explain why there is less D_2 re-emission at this temperature than at 800 K. The general trend of the ratio of C-bonded/all D shows that heating/annealing of the sample increases this number. This is because D_2 is emitted while the number of C-bonded D stays the same (for 600 K) or increases (for 800 and 1000 K).

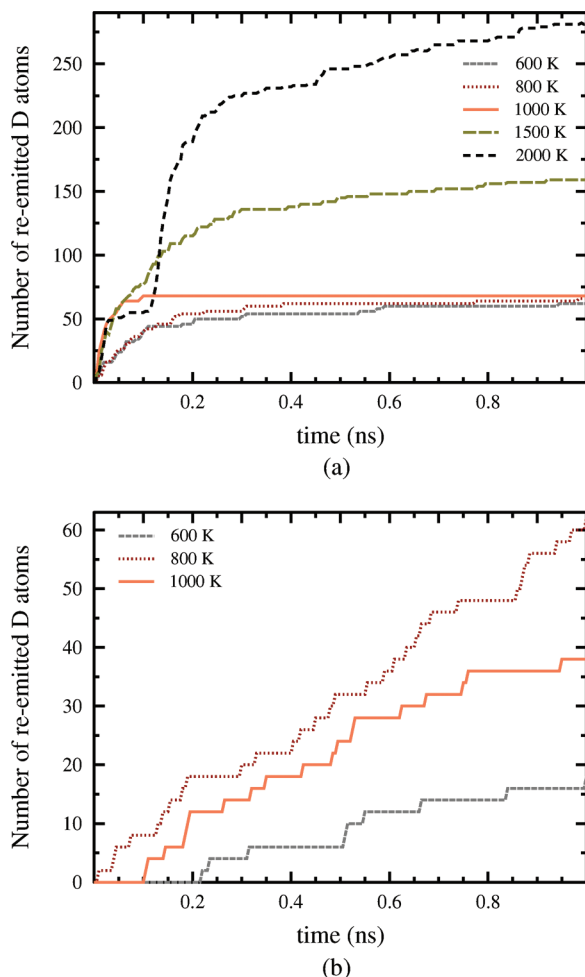


Figure 6. D re-emission versus time: annealing of the sample after 5000 impacts with 100% D (a) and 90% D, 10% C (b). The ion energy was 100 eV during bombardment.

TABLE 3: Number n of Re-emitted Atomic D and D_2 after Annealing for 1 ns at 600–2000 K^a

	600 K	800 K	1000 K	1500 K	2000 K
n D molecules	31	33	33	74	115
n atomic D	0	0	2	11	52
n all re-emitted D	62	66	68	159	282

^a Input for the annealing simulation was from the cell after 5000 impacts with 100 eV pure D containing 430 D atoms (for further structure details, see Tables 1 and 2).

The reason why the D re-emission behavior for the pure D and mixed C bombarded samples is so different is likely due to the fact that first, there is more C present in the C mixed bombarded sample, and second, this carbon is more evenly distributed on the surface, while most of the surface carbon was eroded during the pure D bombardment, leading to a tungsten-rich top. Therefore, we can speculate that in this tungsten-rich top, not so much carbon is present, which traps D during heating.

Since during the 300 eV 90% D, 10% Ar bombardment a relatively large D_2 re-emission yield was obtained (Figure 5b), also this sample was annealed for 1 ns after bombardment. However, no further D re-emission was found for annealing temperatures of 600–1000 K. Only one Ar atom was re-emitted during those simulations.

Wang et al.¹ reported re-emission in the form of D_2 and CD_4 during 1.5 keV D^+ bombardment from $W_{60}C_{40}$ with a flux of $\sim 10^{19} \text{ m}^{-2} \text{ s}^{-1}$ at room temperature. That the CD re-emission

TABLE 4: Number n of Re-emitted and Trapped D and C-Bonded D after Annealing for 1 ns at 600–1000 K^a

	600 K, initial	600 K, 1 ns	800 K, 1 ns	1000 K, 1 ns
n D_2 molecules in sample	109	101	80	92
n re-emitted D molecules		9	31	19
n re-emitted atomic D		0	0	0
n all re-emitted D		18	62	38
n C-bonded D	153	153	158	169
n all D in sample	493	475	431	455
ratio D_2 /all D (%)	42.22	42.53	37.12	40.44
ratio C-bonded/all D (%)	31.03	32.21	36.66	37.142

^a Input for the annealing simulation was from the cell after 5000 impacts with 100 eV of 90% D, 10% C containing 493 D atoms (for further structure details, see Tables 1 and 2). For comparison, the data before heating is added.

was zero at very low fluence¹ agrees with our simulation result, where we saw no CD_4 re-emission.

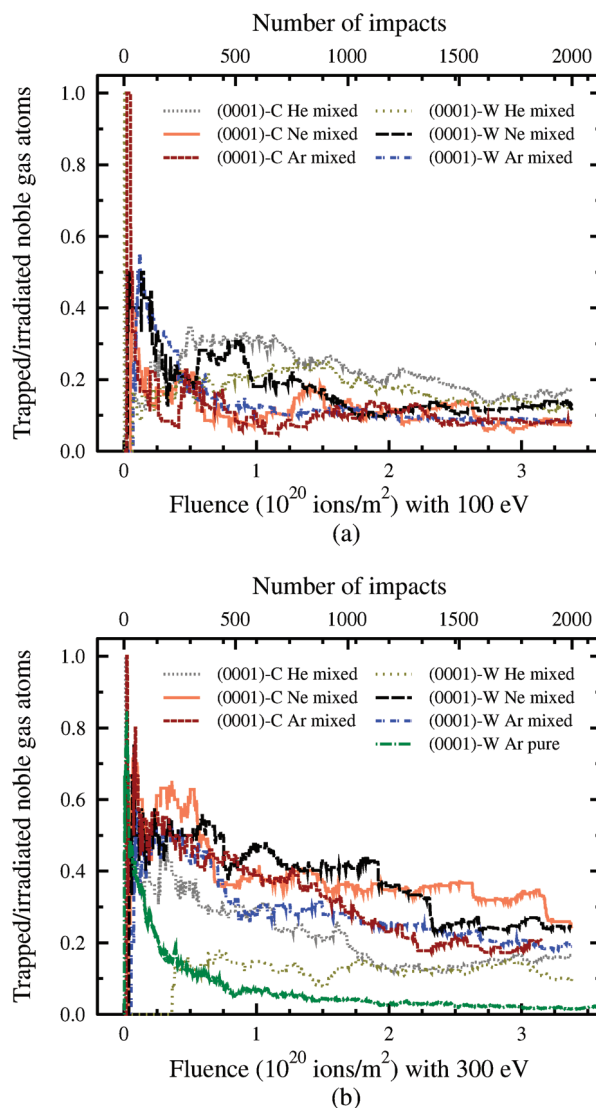


Figure 7. The ratio of trapped over incident noble gas atoms in the sample for 90% D, 10% He, Ne, or Ar bombardment for (a) 100 and (b) 300 eV. In (b), the trapping ratio for 100% (pure) Ar bombardment on W-terminated WC is added.

TABLE 5: Noble Gas Atom Reflection Ratio (the Number of Reflected over the Number of Incident Noble Gas Atoms) and Implantation Ratio (the Number of Noble Gas Atoms Implanted Through Sample over the Number of Incident Noble Gas Atoms) after a Fluence of 3.38×10^{20} ions/ m^{-2} ^a

	(0001)-C, He	(0001)-W, He	(0001)-C, Ne	(0001)-W, Ne	(0001)-C, Ar	(0001)-W, Ar	(0001)-W, Ar pure
ion energy (eV)	100	100	100	100	100	100	
reflection ratio (%)	80	83	92	88	92	92	
implantation ratio (%)	3.1	3.4	0.5	0	0	0	
ion energy (eV)	300	300	300	300	300	300	300
reflection ratio (%)	50	52	74	75	79	81	98
implantation ratio (%)	33	38	2	0.5	0.6	0.5	0.1

^a Always, data on mixed bombardment (90% D and 10% noble gas ion) are given unless otherwise specified.

Experimental results show that most of the retained D in WC above 573 K is bound by carbon.⁴ This trend is also seen in our simulation since the number of C-bonded D increases the more that D is re-emitted from the sample (Table 4).

We summarize that D₂ re-emission during bombardment was dominantly seen for 100 eV bombardment. Moreover, during the annealing simulations after bombardment, D re-emission was only seen for 100 eV bombarded samples. The D₂ re-emitted during this process was present dominantly as molecules in the sample before emission. No D₂ formation on the surface was observed. D₂ was highly mobile in WC.

Accumulation of Noble Gas in the Sample. The ratio of the number of trapped noble gas atoms in the sample over the number of incident noble gas atoms during the 90% D, 10% He, Ne, or Ar bombardment with ion energies of 100 and 300 eV is illustrated in Figure 7. For comparison, the 300 eV 100% Ar is added in Figure 7b. More noble gas was accumulated in the 300 eV bombarded samples than in the 100 eV bombarded one, which is indicated by a higher trapping ratio in Figure 7a than that in (b). Moreover, the trapping ratio decreased during prolonged bombardment for both 100 and 300 eV due to the formation of a tungsten-rich surface layer (since C is preferably sputtered), which has a higher reflection probability for the impinging noble gas atoms.

The reason for the different accumulation behavior for He, Ne, and Ar at 100 and 300 eV in Figure 7 is discussed in the following. For that reason, the reflection/re-emission of noble gas during irradiation and the noble gas atoms which were implanted through the *z* dimension of the sample during irradiation (which were discarded in further calculations) were counted. These reflection and implantation ratios per incident noble gas atom are given in Table 5. As seen in the table, the reflection ratios for 300 eV are smaller than those for 100 eV, and therefore, more noble gas is accumulated in the 300 eV bombarded samples. Comparing the implantation ratio for He for 100 and 300 eV explains why there is less He accumulated for 300 eV than for 100 eV. The implantation ratios for He are 3.1 and 3.4% for 100 eV, while they are 33 and 38% for 300 eV, meaning more than 30% of the incident He is implanted deeper than the *z* boundary of the simulation cell and therefore discarded from the cell. The implantation ratios are only very small for Ne and Ar and do not differ that dramatically for 100 and 300 eV.

In pure tungsten, He bombardment leads to the formation of He clusters/bubbles, which can erupt if they are near the surface.³³ However, analyzing the structure showed no clustering or bubble formation of the noble gas atoms in the sample in our simulations. The noble gas atoms were spread out within the sample, also in the 100% Ar bombardment. We want to comment that because, for 300 eV He bombardment, more than 30% of the incident He was implanted deeper than the cell

boundaries (Table 5), much larger simulation cells than those in this present study would be needed to clarify He bubble formation in tungsten carbide.

To sum up, we may say that, depending on the ion energy, noble gas was accumulated in the sample at different ratios. No noble gas clusters were observed at our simulated fluence.

Conclusions

MD simulations of deuterium cobombardment with impurities on crystalline tungsten carbide were carried out to study deuterium trapping and re-emission. Up to 5000 impacts with ion energies from 100 to 300 eV were performed, corresponding to a fluence of 8.45×10^{20} m^{-2} . The ion flux was 3.38×10^{28} m^{-2} s^{-1} . We conclude the following.

(i) D bombardment with and without impurities changes the structure from crystalline to amorphous. The “gradual amorphization” process has been observed by RBS in other materials. The MD results are directly for so low temperatures or so high fluxes that no significant defect migration occurs.

(ii) D trapping can lead to a “blistering/flaking”-like effect. If a steady-state D concentration is reached, the force it exerts due to the D₂ gas pressure can lead to a rupture in the sample. This mechanism is the consequence of the high fluxes in the simulations. It is not responsible for blisters seen in experiments that are related to diffusion processes and where fluxes are orders of magnitude lower.

(iii) D₂ re-emission after annealing to 600–1000 K showed that D₂ is highly mobile in tungsten carbide. Hence, for annealing for longer time scales than those considered here, most D in the form of D₂ would leave the sample, and then, most of the trapped D would be bonded to C. Thus, the concentration of C in WC determines the amount of trapped D.

(iv) The noble gas atoms did not form clusters in our simulations. To study He clustering by ion bombardment in WC, larger simulation cells and higher fluences than those here would be needed.

(v) No direct comparison of the MD simulations to experiment was possible since the MD fluxes were orders of magnitude higher and the fluence was much lower than those in experiments. However, mixed ion beam experiments on WC using high (experimental) fluxes could validate our results and bring more insight to the mechanisms.

To obtain a full picture of what happened during the bombardment, the interested reader is referred to ref 32, which deals with sputtering and discusses bond breaking.

Acknowledgment. This work, supported by the European Communities under the contract of Association between EURATOM and Tekes, was carried out within the framework of the European Fusion Development Agreement. The research

was performed within the Finnish Centre of Excellence in Computational Molecular Science (CMS), financed by the Academy of Finland and the University of Helsinki.

References and Notes

- (1) Wang, W.; Alimov, V. K.; Scherzer, B. M. U.; Roth, J. *J. Nucl. Mater.* **1997**, *241–243*, 1087–1092.
- (2) Alimov, V. *Phys. Scr.* **2004**, *T108*, 46–56.
- (3) Kimura, H.; Nishikawa, Y.; Nakahata, T.; Oyaidzu, M.; Oya, Y.; Okuno, K. *Fusion Eng. Des.* **2006**, *81*, 295–299; Proceedings of the Seventh International Symposium on Fusion Nuclear Technology, ISFNT-7 Part A.
- (4) Igarashi, E.; Nishikawa, Y.; Nakahata, T.; Yoshikawa, A.; Oyaidzu, M.; Oya, Y.; Okuno, K. *J. Nucl. Mater.* **2007**, *363–365*, 910–914; Plasma-Surface Interactions-17.
- (5) Parker, R.; Janeschitz, G.; Pacher, H.; Post, D.; Chiochio, S.; Federici, G.; Ladd, P.; Team, I. J. C.; Teams, H. *J. Nucl. Mater.* **1997**, *241–243*, 1–26.
- (6) Garrison, B. J.; Goddard, W. A., III *Phys. Rev. B* **1987**, *36*, 9805.
- (7) Schoolcraft, T. A.; Garrison, B. J. *J. Am. Chem. Soc.* **1991**, *113*, 8221.
- (8) Feil, H.; Dieleman, J.; Garrison, B. J. *J. Appl. Phys.* **1993**, *74*, 1303–9.
- (9) Barone, M. E.; Graves, D. B. *J. Appl. Phys.* **1995**, *78*, 6604.
- (10) Salonen, E.; Nordlund, K.; Keinonen, J.; Wu, C. H. *Phys. Rev. B* **2001**, *63*, 195415.
- (11) Harper, J. M. E. Ion Beam Etching. In *Plasma Etching - An Introduction*; Manos, D. M., Flamm, D. L., Eds.; Academic Press: San Diego, CA, 1989.
- (12) Nordlund, K.; Salonen, E.; Krashennikov, A. V.; Keinonen, J. *Pure Appl. Chem.* **2006**, *78*, 1203–1212.
- (13) The definitions of sputter etching and direct abstractive etching do not explicitly state whether they are endo- or exothermal.
- (14) Condon, J. B.; Schober, T. *J. Nucl. Mater.* **1993**, *207*, 1–24.
- (15) Alimov, V.; Komarov, D. *J. Nucl. Mater.* **2003**, *313–316*, 599–603; Plasma-Surface Interactions in Controlled Fusion Devices 15.
- (16) Ogorodnikova, O.; Roth, J.; Mayer, M. *J. Nucl. Mater.* **2003**, *313–316*, 469–477; Plasma-Surface Interactions in Controlled Fusion Devices 15.
- (17) Shimada, T.; Ueda, Y.; Nishikawa, M. *Fusion Eng. Des.* **2003**, *66–68*, 247–251; 22nd Symposium on Fusion Technology.
- (18) Alimov, V.; Roth, J.; Causey, R.; Komarov, D.; Linsmeier, C.; Wiltner, A.; Kost, F.; Lindig, S. *J. Nucl. Mater.* **2008**, *375*, 192–201.
- (19) Fukumoto, M.; Ohtsuka, Y.; Ueda, Y.; Taniguchi, M.; Kashiwagi, M.; Inoue, T.; Sakamoto, K. *J. Nucl. Mater.* **2008**, *375*, 224–228.
- (20) Enomoto, N.; Muto, S.; Tanabe, T.; Davis, J.; Haasz, A. *J. Nucl. Mater.* **2009**, *385*, 606–614.
- (21) Shu, W.; Kawasuso, A.; Yamanishi, T. *J. Nucl. Mater.* **2009**, *386–388*, 356–359; Fusion Reactor Materials, Proceedings of the 13th International Conference on Fusion Reactor Materials.
- (22) Träskelin, P.; Juslin, N.; Erhart, P.; Nordlund, K. *Phys. Rev. B* **2007**, *75*, 174113.
- (23) The target conditions are those of a W baffle at medium temperatures.³⁴
- (24) Nordlund, K. *Parcas Computer Code*; University of Helsinki: Helsinki, Finland, 2006. The main principles of the molecular dynamics algorithms are presented in refs 35 and 36. The adaptive time step and electronic stopping algorithms are the same as in ref 37.
- (25) Juslin, N.; Erhart, P.; Träskelin, P.; Nord, J.; Henriksson, K. O. E.; Nordlund, K.; Salonen, E.; Albe, K. *J. Appl. Phys.* **2005**, *98*, 123520.
- (26) Ziegler, J. F.; Biersack, J. P.; Littmark, U. *The Stopping and Range of Ions in Matter*; Pergamon: New York, 1985.
- (27) Berendsen, H. J. C.; Postma, J. P. M.; van Gunsteren, W. F.; DiNola, A.; Haak, J. R. *J. Chem. Phys.* **1984**, *81*, 3684.
- (28) Allen, M. P.; Tildesley, D. J. *Computer Simulation of Liquids*; Oxford University Press: Oxford, England, 1989.
- (29) Lohner, T.; Kotai, E.; Khanh, N.; Toth, Z.; Fried, M.; Vedam, K.; Nguyen, N.; Hanekamp, L.; van Silfhout, A. *Nucl. Instrum. Methods Phys. Res., Sect. B* **1994**, *85*, 335–339.
- (30) Kucheyev, S.; Williams, J.; Jagadish, C.; Zou, J.; Li, G. *Phys. Rev. B* **2000**, *62*, 7510–7522.
- (31) Nakajima, K.; Toyofuku, H.; Kimura, K. *Jpn. J. Appl. Phys.* **2001**, *40*, 2119–2122.
- (32) Vörtler, K.; Björkas, C.; Nordlund, K. 2010, to be published.
- (33) Henriksson, K. O. E.; Nordlund, K.; Keinonen, J. *Nucl. Instrum. Methods Phys. Res., Sect. B* **2005**, *244*, 377–391.
- (34) Loarte, A.; Federici, G. 2006; private communication.
- (35) Nordlund, K.; Ghaly, M.; Averbach, R. S.; Caturla, M.; Diaz de la Rubia, T.; Tarus, J. *Phys. Rev. B* **1998**, *57*, 7556–7570.
- (36) Ghaly, M.; Nordlund, K.; Averbach, R. S. *Philos. Mag. A* **1999**, *79*, 795.
- (37) Nordlund, K. *Comput. Mater. Sci.* **1995**, *3*, 448.